J|A|C|S
ARTICLES
Published on Web 09/25/2004

Electronic Modulation of Dithienothiophene (DTT) as π-Center of D-π-D Chromophores on Optical and Redox Properties: Analysis by UV−Vis−NIR and Raman Spectroscopies Combined with Electrochemistry and Quantum Chemical DFT Calculations

Rocío Ponce Ortiz,[†] Mari Carmen Ruiz Delgado,[†] Juan Casado,[†] Víctor Hernández,[†] Oh-Kil Kim,[‡] Han Young Woo,[‡] and Juan T. López Navarrete*[,†]

Contribution from the Departamento de Química Física, Facultad de Ciencias, Universidad de Málaga, 29071-Málaga (Spain) and Chemistry Division, Naval Research Laboratory, Washington, DC, 20375-5342

Received May 19, 2004; E-mail: teodomiro@uma.es

Abstract: In this paper, we study three symmetrical D-π-D chromophores containing dithieno[3,2-*b*:2′,3′-*d*]thiophene (DTT) as the π-center and various donor end moieties, by means of UV−vis−NIR and FT-Raman spectroscopy and in situ spectroelectrochemistry. The compounds display dual redox properties: all exhibited two oxidations and single stable reduction peaks contrarily to the one or two oxidations and none reduction which could be anticipated in view of their chemical structures. We analyze the possible electronic modulation by the π-conjugated DTT relay in the redox process and electronic coupling between the two electron donor (D) units attached through conjugation to opposite sides of the π-linker. To this end, the UV−vis−NIR and FT-Raman spectra of the neutral compounds and of the charged species generated upon in situ p- or n-doping have been recorded and interpreted with the help of Density Functional Theory (DFT) calculations. The analysis of the peculiar Raman features of these π-conjugated chromophores is guided by the formalism of the Effective Conjugation Coordinate (ECC) theory. This research shows that the Raman spectroscopic characterization of this type of D-π-D structures is a powerful tool to derive information about their π-conjugational properties in the pristine and doped states.

I. Introduction

Oligothiophenes are ideal models for π-conjugated electrically conducting polymers.[1,2] and novel molecular materials for all-organic field-effect transistors[3,4] and light-emitting devices.[5,6] Oligothiophenes are therefore particularly appealing building blocks for using as electron relay (π-center) or mediator to enhance or modulate the electronic properties of π-conjugated molecules. As a model approach toward electronic property modulation, chromophore sequences are arranged in such a way that electron-donor (D) and/or acceptor (A) units are linked through π-conjugation to a central electron relay at the ends.[7] The study of the electronic properties of such structures provide valuable information for understanding of relay role of the π-center and for developing functional tuning and enhancing the efficiency of electronic/photonic materials. The well-recognized efficiency of oligothiophenes as property modulator is associated to the lower resonance energy as compared to benzene (and to the ability of sulfur d orbitals to mix well with aromatic π-orbitals),[8,9] such that electron-transfer through the π-center between the end moieties is facilitated, thereby anticipating a pronounced alteration in electronic/photonic properties. The conjugational interactions between the end chromophores could be even enhanced if rigid π-centers are used. This is noticeable when the end groups are redox-active moieties.[10] A fact that evidences the effective role of fused thiophenes as relays is that their longest wavelength absorptions exhibit and excellent linear correlation with the number of thiophene rings up to five.[11]

Vis-NIR electronic absorption and infrared and Raman spectroscopies have been used from the discovery of the electrically conducting polymers to characterize many different

[†] Universidad de Málaga.
[‡] Naval Research Laboratory.

(1) Tourillon, G. *Handbook of Conducting Polymers*; Dekker: New York, 1986; p 293.
(2) Baüerle, P. *Electronic Materials: The Oligomeric Approach*; Wiley-VCH: Weinheim, 1998; p 105.
(3) Garnier, F.; Horowitz, G.; Fichou, D.; Yassar, A. *Synth. Met.* **1996**, *81*, 163.
(4) Li, X.-C.; Sirringhaus, H.; Garnier, F.; Holmes, A. B.; Moratti, S. C.; Feeder, N.; Clegg, W.; Teat, S. M.; Friend, R. H. *J. Am. Chem. Soc.* **1998**, *120*, 2206.
(5) Geiger, F.; Stoldt, M.; Baeuerle, P.; Scheizer, H.; Umbach, E. *Adv. Mater.* **1993**, *5*, 922.
(6) Gill, R. E.; Malliaras, G. G.; Wildeman, J.; Hadziioannou, G. *Adv. Mater.* **1994**, *6*, 132.
(7) Kim, O.-K.; Fort, A.; Bazoukas, M.; Blanchard-Desce, M.; Lehn, J.-M. *J. Mater. Chem.* **1999**, *9*, 2227.
(8) Moreira, I. S.; Franco, D. W. *J. Chem. Soc. Chem. Commun.* **1992**, 450.
(9) Takahashi, K.; Nihira, T.; Akiyama, K.; Ikegami, Y.; Fukuyo, E. *J. Chem. Soc. Chem. Commun.* **1992**, 620.
(10) (a) Kim, O.-K.; Woo, H. Y.; Kim, J. K.; Heuer, W. B.; Lee, K.-S.; Kim, C. Y. *Chem. Phys. Lett.* **2002**, *364*, 432. (b) Kim, O.-K.; Lee, K.-S.; Woo, H. Y.; Kim, K.-S.; He, G. S.; Swiatkiewicz, J.; Prasad, P. N. *Chem. Mater.* **2000**, *12*, 284.
(11) Mazaki, Y.; Kobayashi, K. *Tetrahedron Lett.* **1989**, *30*, 3315.

classes of π-conjugated oligomers and polymers; and among them Raman spectroscopy has been shown to be of great help in the following: (i) estimating the degree of π-conjugation in neutral state,[12−14] (ii) characterizing different types of conjugational defects in doped materials,[15] and (iii) analyzing the efficiency of the intramolecular charge transfer in push−pull π-conjugated systems.[16,17] The appearance of only a few and overwhelmingly strong Raman bands, even for systems with complex chemical structures, is a direct consequence, on the basis of the Effective Conjugation Coordinate (ECC) theory,[18] of the existence of a rather effective electron−phonon coupling over the whole quasi one-dimensional π-backbone. In aromatic and heteroaromatic polyconjugated systems, the so-termed as *collective ECC vibrational coordinate* has the analytic form of a linear combination of ring C=C/C−C stretchings which points in the direction from the benzenoid structure (usually that of the ground state) to the quinonoid structure (that corresponding to the electronically excited state or the charged species). ECC theory states that upon increasing conjugation length (CL), the totally symmetric vibrational normal modes of the neutral system mostly involved in the lattice dynamics of the ECC coordinate (namely, those which give rise to the few and rather strong Raman bands experimentally observed) undergo sizable dispersions both in frequency and intensity. Thus, changes in the peak positions and relative intensities of the Raman features with increasing chain length are particularly useful in evaluating the *mean conjugation length* for the members of a given series of neutral oligomers. On the other hand, when π-conjugated oligomers and, in particular, aromatic oligothiophenes become oxidized (either chemically or electrochemically), various types of quinonoid-like charged defects are created.[19] These structural modifications also induce a significant redshift of the Raman lines associated to the π-conjugated path (due the softening of the C=C bonds). The Raman spectral differences between the neutral and doped forms of a π-conjugated compound are an useful tool for elucidating the type of charged carriers created upon oxidation.[12−15]

Here, we analyze, by means of FT-Raman and vis-NIR spectroscopies aided by Density Functional Theory (DFT) model chemistry, the electrochemical modulation of dithieno[3,2-*b*:2′,3′-*d*]thiophene (DTT) as relay in some D-π-D structures bearing three different types of donor end moieties.[20,10] The comparison between the optical absorptions and vibrational features of the neutral and doped forms of each chromophore sequence should provide useful information about the role of the DTT π-bridge in the redox process and electronic coupling of the end D/D pairs. DFT calculations are performed as a guide for the analysis of the electrochemical and spectroscopic data, both in neutral and doped states, and to derive relevant molecular parameters such as bond lengths and angles, Molecular Orbital (MO) topologies, and atomic charge distributions.

II. Results and Discussion

A. UV−Vis Absorption Data. The chemical structures and abbreviate notation of the various compounds studied in this article are depicted in Figure 1 and their absorption and emission spectra are displayed in Figure 2. The chromophores show high solubility, and their spectral features are concentration independent in the range examined, suggesting that the molecules are not in an aggregated phase.

All of the chromophores have the strongest absorption band around 450 nm, which display a well-resolved vibronic structure at room temperature (i.e., which is particularly evident in the case of the symmetric D-π-D systems). The absorption maxima, λ_{max}, of the compounds with various components are summarized in Table 1. This result suggests that there exists a high degree of intramolecular conformational order (even under solution), in this type of D-π-D systems; more specifically, a large correspondence between the ground and excited state's geometries, which should result in a nearly flat arrangement or full coplanarization of the three constituting moieties, and hence in an enhanced π-electron delocalization.

B. Optimized Geometries and Electronic Spectra of Neutral Compounds. To gain a deeper insight into the changes on the molecular structure and equilibrium charge distribution induced by the attachment of various D/D pairs at the end α,ω-positions of the DTT π-center, we have performed geometry optimizations, within the framework of the Density Functional Theory, for **DTT**, **D_1-DTT-D_1**, **D_2-DTT-D_2**, **D_3-DTT-D_3**, and **D_3-DTT** by using ab initio B3LYP/3-21G* model chemistry (the main skeletal bond lengths for the neutral forms of all these compounds are summarized in Table 2). Prior to the optimization geometries, we performed a ^{1}H NMR study of the chromophores in $CDCl_3$ to assess information about the preferred molecular conformation. The coupling constant (~14 Hz) between the two hydrogens of the vinylenic bridges confirms the all-anti arrangement of the π-center and the D/D pair to be the most stable conformer both for both the neutral and dicationic species (i.e., this structure was assumed in all calculations).

(12) Sakamoto, A.; Furukawa, Y.; Tasumi, M. *J. Phys. Chem.* **1994**, *98*, 4635.
(13) (a) Yokonuma, N.; Furukawa, Y.; Tasumi, M.; Kuroda, M.; Nakayama, J. *Chem. Phys. Lett.* **1996**, *255*, 431. (b) Harada, I.; Furukawa, Y. *Vibrational Spectra and Structure*; Durig, J., Ed.; Elsevier: Amsterdam, 1991; Vol. 19, p 369.
(14) (a) Hernandez, V.; Casado, J.; Ramirez, F. J.; Zotti, G.; Hotta, S.; Lopez Navarrete, J. T. *J. Chem. Phys.* **1996**, *104*, 9271. (b) Casado, J.; Hernandez, V.; Hotta, S.; Lopez Navarrete, J. T. *J. Chem. Phys.* **1998**, *109*, 10419. (c) Moreno Castro, C.; Ruiz Delgado, M. C.; Hernandez, V.; Hotta, S.; Casado, J.; Lopez Navarrete, J. T. *J. Chem. Phys.* **2002**, *116*, 10419. (d) Moreno Castro, C.; Ruiz Delgado, M. C.; Hernandez, V.; Shirota, Y.; Casado, J.; Lopez Navarrete, J. T. *J. Phys. Chem. B* **2002**, *106*, 7163.
(15) (a) Casado, J.; Hernandez, V.; Hotta, S.; Lopez Navarrete, J. T. *J. Chem. Phys.* **1998**, *109*, 10419. (b) Casado, J.; Hernandez, V.; Hotta, S.; Lopez Navarrete, J. T. *Adv. Mater.* **1998**, *10*, 1258. (c) Casado, J.; Miller, L. L.; Mann, K. R.; Pappenfus, T. M.; Kanemitsu, Y.; Orti, E.; Viruela, P. M.; Pou-Amerigo, P.; Hernandez, V.; Lopez Navarrete, J. T. *J. Phys. Chem. B* **2002**, *106*, 3872. (d) Casado, J.; Miller, L. L.; Mann, K. R.; Pappenfus, T. M.; Hernandez, V.; Lopez Navarrete, J. T. *J. Phys. Chem. B* **2002**, *106*, 3597. (e) Casado, J.; Ruiz Delgado, M. C.; Shirota, Y.; Hernandez, V.; Lopez Navarrete, J. T. *J. Phys. Chem. B* **2003**, *107*, 2637.
(16) (a) Hernández, V.; Casado, J.; Effenberger, F.; López Navarrete, J. T. *J. Chem. Phys.* **2000**, *112*, 5105. (b) Casado, J.; Hernández, V.; Kim, O.-K.; Lehn, J.-M.; López Navarrete, J. T.; Delgado Ledesma, S.; Ponce Ortiz, R.; Ruiz Delgado, M. C.; Vida, Y.; Perez-Inestrosa, E. *Chem. Eur. J.* **2004**, *10*, 3805.
(17) (a) Gonzalez, M.; Segura, J. L.; Seoane, C.; Martin, N.; Garin, J.; Orduna, J.; Alcala, R.; Villacampa, B.; Hernandez, V.; Lopez Navarrete, J. T. *J. Org. Chem.* **2001**, *66*, 8872. (b) Casado, J.; Pappenfus, T. M.; Miller, L. L.; Mann, K. R.; Orti, E.; Viruela, P. M.; Pou-Amerigo, P.; Hernandez, V.; Lopez Navarrete, J. T. *J. Am. Chem. Soc.* **2003**, *125*, 2534.
(18) (a) Zerbi, G.; Castiglioni, C.; Del Zoppo, M. *Electronic Materials: The Oligomer Approach*; Wiley-VCH: Weinheim, 1998; p 345. (b) Castiglioni, C.; Gussoni, M.; Lopez Navarrete, J. T.; Zerbi, G. *Solid State Commun.* **1988**, *65*, 625. (c) Lopez Navarrete, J. T.; Zerbi, G. *J. Chem. Phys.* **1991**, *94*, 957 and 965. (d) Hernandez, V.; Castiglioni, C.; Del Zoppo, M.; Zerbi, G. *Phys. Rev. B* **1994**, *50*, 9815. (e) Agosti, E.; Rivola, M.; Hernandez, V.; Del Zoppo, M.; Zerbi, G. *Synth. Met.* **1999**, *100*, 101. (f) Zerbi, G. *Handbook of Conducting Polymers*; Marcel Dekker: New York, 1998.
(19) (a) Ehrendorfer, Ch.; Karpfen, A. *J. Phys. Chem.* **1994**, *98*, 7492. (b) Ehrendorfer, Ch.; Karpfen, A. *J. Phys. Chem.* **1995**, *99*, 5341.
(20) (a) Kim, O.-K.; Lee, K.-S.; Huang, Z.; Heuer, W. B.; Paik-Sung, C. S. *Opt. Mater.* **2002**, *21*, 559. (b) Kim, O.-K.; Woo, H. Y.; Lee, K.-S.; Kim, J. K.; Kim, D. Y.; Shim, H.-K.; Kim, C. Y. *Synth. Met.* **2001**, *121*, 1607.

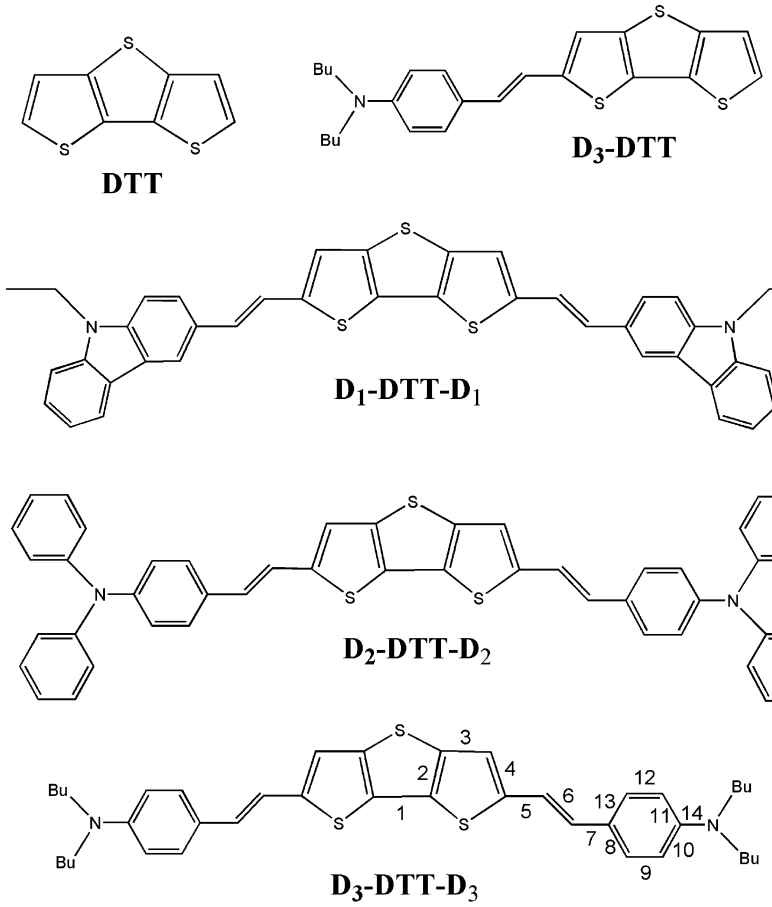

Figure 1. Chemical structures of the compounds and abbreviate notation to be used throughout the text (bond numbering is to be used for Table 2).

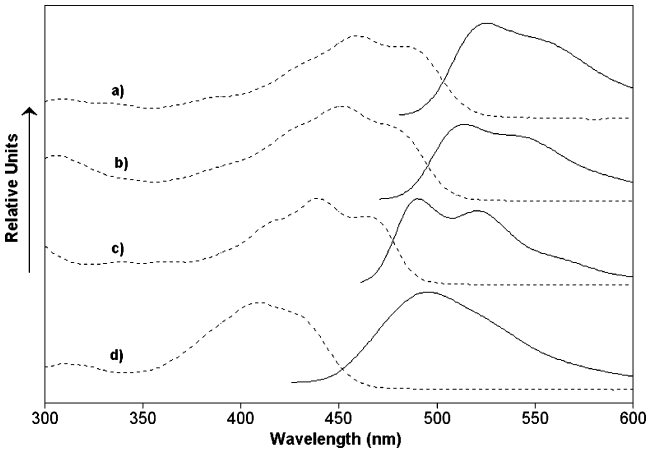

Figure 2. Normalized absorption (dashed lines) and emission (solid lines) spectra of (a) **D_3-DTT-D_3**, (b) **D_2-DTT-D_2**, (c) **D_1-DTT-D_1**, and (d) **D_3-DTT** in CH_2Cl_2 solution. The emission spectra are obtained by exciting at the maximum of the absorption spectrum.

Table 1. UV-Vis Absorption Maxima (λ_{max}) of the Compounds in CH_2Cl_2 Solution

compd	λ_{max} (nm) (in CH_2Cl_2)
D_1-DTT-D_1	391, 419, 439, and 464
D_2-DTT-D_2	393, 429, 450, and 474
D_3-DTT-D_3	386, 430, 459, and 484
D_3-DTT	408 and 429

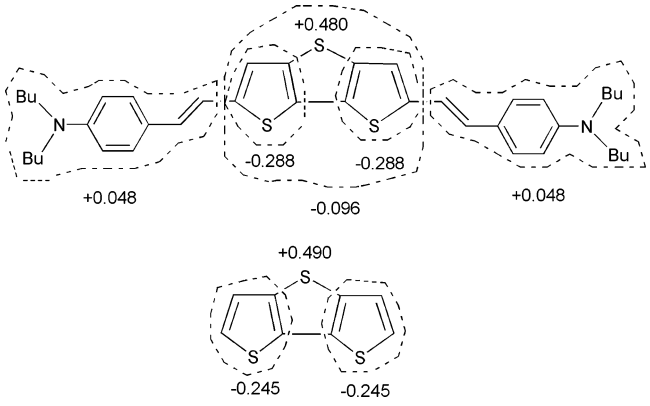

Figure 3. Overall summation (in *e*) of the B3LYP/3-21G* natural population analysis (NPA) atomic charges on different molecular domains for **DTT** and **D_3-DTT-D_3**.

In view of the theoretical data, one observes that the skeletal bonds at the central part of each **D_n-DTT-D_n** (n = 1, 2, or 3) chromophore display nearly the same length than their counterparts in the other two symmetrically disubstituted systems, so that the structure of the conjugated C═C/C−C path between the two nitrogen atoms of each chromophore is almost identical in the three cases. We also observe, from the comparison of the B3LYP/3-21G* optimized geometries of **D_3-DTT-D_3** and **D_3-DTT**, that the structural changes induced by the attachment of a single donor group to the **DTT** π-center are quite similar to those taking place upon the symmetric disubstitution, but for the most remote thienyl ring (i.e., the unsubstituted end thienyl ring), whose geometry little changes with respect to **DTT**.

For **D_1-DTT-D_1**, the mean single-double CC bond length alternation pattern (BLA) of the thienyl rings covalently attached

Table 2. Selected DFT//B3LYP/3-21G* Skeletal Bond Lengths (in Å) for the Neutral Forms of **DTT**, **D_1-DTT-D_1**, **D_2-DTT-D_2**, and **D_3-DTT-D_3**

bond	DTT	D_1-DTT-D_1	D_2-DTT-D_2	D_3-DTT-D_3	D_3-DTT
1	1.422	1.414	1.414	1.414	1.419
2	1.399	1.403	1.404	1.403	1.402
3	1.427	1.416	1.415	1.416	1.417
4	1.369	1.385	1.386	1.386	1.385
5		1.441	1.440	1.440	1.447
6		1.352	1.353	1.354	1.353
7		1.462	1.459	1.456	1.458
8		1.419	1.410	1.408	1.411
9		1.389	1.388	1.386	1.384
10		1.397	1.406	1.417	1.419
11		1.428	1.409	1.419	1.416
12		1.390	1.386	1.383	1.386
13		1.408	1.411	1.411	1.410
14		1.394	1.421	1.382	1.380

through the vinylene bridges to the donor end groups amount to 0.022 Å; whereas the corresponding values for the other chromophores are as follows: 0.020 Å (**D_2-DTT-D_2**), 0.022 Å (**D_3-DTT-D_3**), and 0.024 and 0.041 Å for the "substituted" and "free" end thienyl rings, respectively, of **D_3-DTT** (or 0.031 Å for the whole π-center, if the CC bond labeled as 1 connecting the two innermost α-positions is also taken into the overall summation). These BLA values, related to the difference between the average length of single and double conjugated CC bonds, can be compared with that of 0.043 Å obtained for **DTT**. Thus, DFT model chemistry evidences that any of the donor end-capping groups studied here gives rise to a similar degree of quinoidization of the **DTT** backbone, being the structural modifications induced by the polarization of the π-electrons cloud quite comparable in the three cases.

A lateral view of the optimized molecular geometry of **D_3-DTT-D_3** shows us that the compound displays a flat structure, what is in agreement with a "sp^2 hybridization" of the nitrogen atoms and the full involvement of their lone pairs in the π-conjugated system.

Figure 3 reports the overall summations of the natural population analysis (NPA) atomic charges on different molecular domains which can be hypothesized within the **DTT** and **D_3-DTT-D_3** systems. B3LYP/3-21G* calculations reveals an interesting feature regarding the "electrostatic picture" of the D-π-D chromophores (as derived from the equilibrium charge distributions of their respective neutral forms): even in the pristine state, the two donor end moieties are slightly charged positively, while the relay is charged negatively twice the amount, as if a weak intramolecular charge transfer (ICT) should take place between the end and central building blocks. On the other hand, we also observe that the outermost thienyl units of the relay are always charged negatively (namely, excluding from the summation in each case the NPA charge on either the C or H atom attached at the end α-positions), whereas the central sulfur is positively charged to a similar amount for all the systems. It follows that the sulfur atom bridging the innermost β-positions of DTT plays a main role in rigidifying the π-center (thus favoring the π-conjugation), but contributes very little to the ICT; this seems to occur in the neutral forms of these D-π-D structures.

To provide insight into the UV−vis absorption spectra of the chromophores in neutral state, TDDFT calculations at the B3LYP/3-21G* level were performed for all the systems.

Table 3. TDDFT//B3LYP/3-21G* Vertical One-Electron Excitations (values in eV) Related to the Strongest Visible Electronic Absorption of **D_1-DTT-D_1**, **D_2-DTT-D_2**, **D_3-DTT-D_3** and **D_3-DTT**

compd	ΔE_{exp} (eV)	$\Delta E_{B3LYP/3-21G^*}$ (eV)	ΔE_{H-L} (eV)	description
D_1-DTT-D_1	2.82	2.59 ($f = 2.49$)	2.82	H → L
D_2-DTT-D_2	2.74	2.39 ($f = 2.45$)	2.65	H → L
D_3-DTT-D_3	2.69	2.52 ($f = 2.22$)	2.71	H → L
D_3-DTT	3.04	3.03 ($f = 1.49$)	3.17	H → L

Transition energies, oscillators strengths, and HOMO−LUMO gaps are listed in Table 3 along with the description of the experimental absorptions in terms of the main one-electron vertical excitations; Figure 4 sketches a diagram with the energies of the molecular orbitals around the gap within the series of compounds, whereas Figure 5 shows the topologies of the frontier MO of **DTT** and **D_3-DTT-D_3**.

As reported in Table 3, the predictions of the TDDFT calculations are in good agreement with the experimental data, and deviations between the measured and calculated excitation energies for the various electronic absorption bands recorded in the visible region (not shown) were of the order 0.1−0.3 eV. As expected, the strongest absorption at around 450 nm is predominantly built up from the HOMO → LUMO excitation. Figure 5 shows that both frontier orbitals spread over the whole π-conjugated backbone, although the largest contributions come from the central part of the chromophores. Regarding the phases of the atomic contributions at the double bonds to both frontier orbitals: in the HOMO the C═C units are π bonding and have an alternating phase with respect to their neighboring C═C units, whereas in the LUMO the "C═C" units are π antibonding and have the same phase as their neighbors. From these calculations, it also becomes apparent that the HOMO and LUMO topologies and sizes are almost identical for the three symmetric **D_n-DTT-D_n** ($n = 1$, 2, or 3) compounds.

From the schematic diagram of the DFT//B3LYP/3-21G* energy levels around the band gap region (Figure 4), we observe that the HOMO and LUMO are stabilized by 0.001 and 0.166 eV, respectively, in going from **D_1-DTT-D_1** to **D_2-DTT-D_2**; whereas their respective energies increase by 0.355 and 0.245 eV, from **D_1-DTT-D_1** to **D_3-DTT-D_3**. Nonetheless, the HOMO−LUMO gap (denoted as ΔE_{H-L} in Table 3) amounts to a similar value for the three systems.

It is noteworthy that the energy of the vertical electronic transition from a doubly occupied MO to a vacant MO is predicted to be smaller than their energy gap, what must be ascribed to the reduced interelectronic interaction upon the single one-electron excitation (i.e., the interaction can be conceptually interpreted in a simple way as the balance between coulomb and exchange terms, and expectedly it should decrease progressively with increasing size of the π-conjugated system). Indeed, the B3LYP/3-21G* HOMO−LUMO energy gaps for the chromophores (ΔE_{H-L} in Table 3) are found to be slightly higher than the TDDFT//B3LYP/3-21G* energies of the corresponding HOMO−LUMO transitions. The fact that the difference between the ΔE_{H-L} and $\Delta E_{B3LYP/3-21G^*}$ values is nearly the same (namely, ∼0.2 eV) for the three symmetrically disubstituted chromophores can be attributed to the great resemblance between the HOMO and LUMO topologies and sizes for these D-π-D structures. It follows that the lowering of the HOMO−LUMO transition energy upon changing the donor D/D pair is

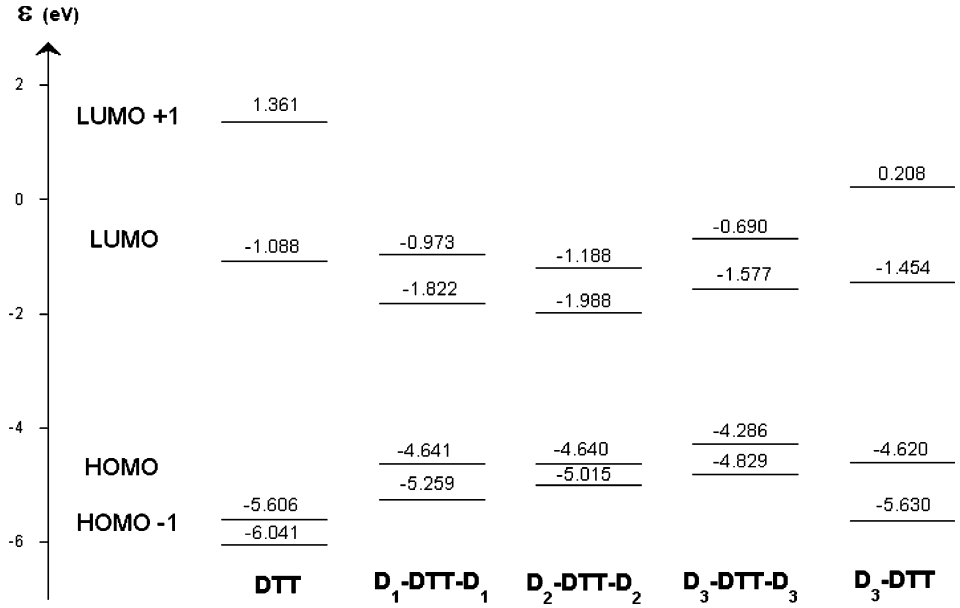

Figure 4. B3LYP/3-21G* one-electron energies (ϵ_i) diagram of the band gap region around the frontiers molecular orbitals of **DTT**, **D_1-DTT-D_1**, **D_2-DTT-D_2**, **D_3-DTT-D_3**, and **D_3-DTT**.

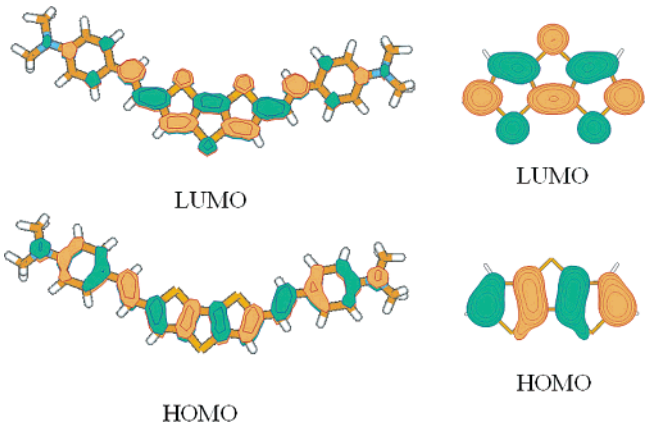

Figure 5. B3LYP/3-21G* electronic density contours (0.03 e/bohr^3) for selected molecular orbitals around the energy gap for the neutral forms of **DTT** and **D_3-DTT-D_3**.

primarily determined by the narrowing of the HOMO−LUMO gap, more than to a significant difference in the energetic balance between the interelectronic interaction terms from one compound to another.

The situation outlined in the preceding paragraphs must be stressed. First, despite being very frequently applied as a direct measure of the HOMO−LUMO gap and the extent of conjugation of a system, UV−vis absorption spectra are not unambiguous in this use. This should also hold when analyzing a homologous series of linear π-conjugated oligomers. It is not infrequent that the optical properties reach saturation already for quite short chain lengths, whereas the orbital energies still continue to change for longer oligomers. As mentioned above, the Coulomb and exchange integrals must decrease with increasing chain length (this trend of variation is in line with the expectation that in more extended systems the electronic repulsion is smaller). However, the narrowing of the HOMO−LUMO gap with increasing number of units in the π-conjugated chain is usually more pronounced, so that the Coulomb and exchange terms play a minor role in determining the energy of the singlet excited-state associated to the HOMO−LUMO transition. As a result, it is desirable that the analysis of the experimental UV−vis data is not based on the spectroscopic intuition only but guided by some type of quantum-chemical calculation about the energies and topologies of the molecular orbitals involved and of the multiconfigurational character of the different absorptions.

As in the case of the absorption spectra, the fluorescence spectra of these choromophores also exhibit a distinct vibronic structure, which becomes more prominent in the symmetrically end-capped D-π-D compounds (see Figure 2). From the approximate spacing of 1200 cm^{-1} it appears that the electronic transition is coupled to a ν(CC) stretching mode; what seems to be in line with the large contribution of the CC bonds at the middle part of the chromophore to the HOMO and LUMO orbitals (Figure 5). In addition, these D-π-D structures display a relatively small Stokes' shift (namely, 1144 cm^{-1} in **D_1-DTT-D_1**; 1642 cm^{-1} in **D_2-DTT-D_2**; and 1613 cm^{-1} in **D_3-DTT-D_3**), revealing that the geometric relaxation upon HOMO−LUMO excitation is rather small.

C. Cyclic Voltammetry. Some electrochemical features of the compounds under study were previously addressed by some of us. However, during the course of the current investigation new interesting and promising electrochemical features have been found, and this section is devoted to their full interpretation in the light of the molecular point of view provided by theoretical calculations.

Figure 6 displays the CV of **D_3-DTT**, **D_3-DTT-D_3**, and **D_2-DTT-D_2**, and Table 4 sums up the potential values recorded in the CV experiments. The monosubstitution of DTT with one **D_3** group significantly lowers the potential of the single irreversible oxidation process of **DTT** (0.93 V) and leads the appearance of a second and stable process at 0.43 V. Both oxidations are associated to the successive generation of the radical cationic and dicationic species.

The first oxidation in **D_3-DTT-D_3** is negatively shifted by 0.16 V with respect to **D_3-DTT**, which is an additional proof of the effective extension of the π-conjugation (i.e., as already revealed by the optical data of the two compounds). Further-

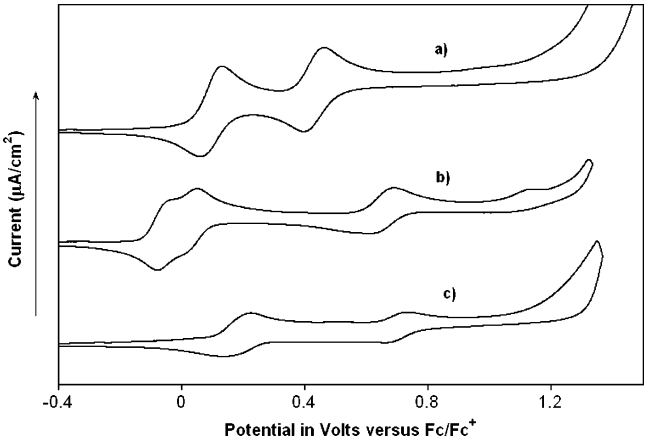

Figure 6. Cyclic voltammograms of (a) **D_3-DTT**, (b) **D_3-DTT-D_3**, and (c) **D_2-DTT-D_2** (in 0.1 mol L^{-1} Bu_4NPF_6/CH_2Cl_2, scan rate 100 mV s^{-1}).

Table 4. Electrochemical Data[a] of D-DTT-D Chromophores with Various D Units

compd	E_{pa}^1 (V)[b]	E_{pa}^2(V)[b]	E_{pa}^3(V)[b]	E_{pa}^4(V)[b]	E_{pr}^1(V)[b]
D_1-DTT-D_1[a]	0.22	0.91			−2.30
D_2-DTT-D_2[a]	0.18 (2e)	0.71	1.2 (i)		−2.20
D_3-DTT-D_3[a]	−0.06	0.04	0.66	1.15 (i)	−2.35
D_3-DTT	0.10	0.43	1.37 (i)		−2.46

[a] Cyclic voltammetry was carried out in 0.1M n-Bu_4NPF_6 in CH_2Cl_2, scan rate 100 mV s^{-1}, glassy carbon as working electrode and a Pt foil as counter-electrode and Ag/Ag^+ electrode as pseudoreference. [b] Potencial values in Volts (V) versus Fc/Fc^+.

more, the potential differences (ΔE) between the first two oxidations are 0.33 V for **D_3-DTT**, 0.10 V for **D_3-DTT-D_3** and 0.00 V for **D_2-DTT-D_2**, since the first two one-electron processes seem to coalesce for **D_2-DTT-D_2** into a single two-electron process. These are clearly related to the Coulombic repulsion between positive charges in the dication. Generally, an increase in effective conjugation leads to a decrease or even cancellation of ΔE. Accordingly, from the electrochemical data alone, the **D_2-DTT-D_2** derivative could be anticipated to be more conjugated than **D_3-DTT-D_3**; but this could not be the real situation from other molecular properties. The unexpected cancellation of ΔE for **D_2-DTT-D_2** could also result from different factors affecting or determining somewhat its molecular and electronic structure. For instance, in view of its chemical structure, it could be anticipated a large tilted conformation between the outermost phenyl rings and the nitrogen atoms of each donor end group, so that the "additional" stabilization, with respect to **D_3-DTT-D_3**, of the lone electron pairs through resonance by part of the aromatic N-substituents is substantially lower than for an "ideal" fully coplanar arrangement of the molecule. This effect is even expected to be acentuated in solution, upon the removal of the solid-state packing forces.

The second oxidation step does not require for a large (or requires only for a rather small) conformational reorganization of the singly oxidized molecule, since, as predicted by the geometry optimization of the radical cation, the first one-electron extraction already induces a sizable degree of planarization and quinoidization in the middle part of the molecule (i.e., between the N atoms). As a result, the second oxidation process takes place at quite similar potential values in **D_2-DTT-D_2** and **D_3-DTT-D_3**, thus justifying for the coalescence of the observed two subsequent one-electron oxidations in **D_3-DTT-D_3** into only one two-electron process in **D_2-DTT-D_2**. For these two related **D_n-DTT-D_n** homologues, additional distinct features due to the successive generation of the radical trication and tetracation appear at high potentials, being the analysis of the corresponding potentials always in agreement with the fact that the **D_3** donor group better accommodates positive charges than **D_2**.

Figure 4, in which the eigenvalues associated to the frontier molecular orbitals are shown, provides a molecular point of view to understand the evolution of the redox processes regarding our D-π-D compounds. Since the energy of the Fc/Fc^+ can be estimated to be −4.80 eV with respect to the vacuum level (i.e., equivalent to our 0.00 V in the CV), it is possible to qualitatively compare the electrochemical potentials with the energies of the frontier orbitals for the neutral system within the Koopman's approach. DFT model chemistry well accounts for the trend of variation of the oxidation potentials. For instance, while the HOMO orbital in **D_3-DTT-D_3** is calculated at −4.29 eV (i.e., which correlates with the −4.74 eV measured for its first oxidation process), the HOMO in **D_2-DTT-D_2** is predicted at −4.64 eV (i.e., in comparison with the −4.98 eV obtained for its first two-electron oxidation). In other words, the HOMO level in **D_3-DTT-D_3** is higher in energy by 0.35 eV than that of **D_2-DTT-D_2**, thus justifying for the anodic shift of the first oxidation of **D_2-DTT-D_2** by 0.24 V regarding its **D_3-DTT-D_3** parent chromophore.

As judging from the high electron-releasing ability of these compounds, as shown by their low or quite low oxidation potentials, one cannot expect these samples to undergo also quasi reversible reduction processes. This finding is rather surprising for this class of chromophores, which are usually regarded as electron-rich π-conjugated systems. It was previously reported the presence of a quasi reversible cathodic process, at −1.50 V, for the dimeric species of DTT, namely α,α′-bis(dithieno-[3,2-*b*:2′,3′-*d*]thiophene).[21] It has also been recently addressed the appearance of reductions for a β-butylsulfanyl substituted sexithiophene.[22] One must therefore ascribe the existence of stable reductions to the electronic modulation by the DTT π-center, although it does not show by itself any redox process at negative potential values. Turning again to the Koopman's approach, the energy of the LUMO orbital for a neutral π-conjugated system can be related with the potential values needed for its reduction. In this regard, our DFT calculations about the energies of frontier OMs give further support for the reasoning of this unexpected electrochemical behavior. As seen in Figure 4, theory qualitatively accounts for the experiments since, for instance, the more stable LUMO term in the series is found for D_2-DTT-D_2, which is related with the lowest energetic reduction at −2.20 V for this molecule along the whole series of chemicals.

The ability of oligothienyl materials to stabilize oxidation states is well-known and explained in terms of the generation of a variety of charged defects able to efficiently delocalize or share the added electrons along the full molecular domain. This requisite is mostly attained in "synthetic metals" through the presence in these systems of long alternating C=C/C−C sequences consisting of quinoid or aromatic structures. Hence, the suitable balance between the two extreme forms leads to

(21) Li, X.-C.; Sirringhaus, H.; Garnier, F.; Holmes, A. B.; Moratti, S. C.; Feeder, N., Clegg, W.; Teat, S. J.; Friend, R. H. *J. Am. Chem. Soc*. **1998**, *120*, 2206.
(22) Alberti, A.; Ballarin, B.; Guerra, M.; Mancciantelli, D.; Mucci, A.; Parenti, F.; Schenetti, L.; Seeber, R.; Zanardi, C. *Chem. Phys. Chem.* **2003**, *4*, 1216.

the stabilization (appearance), or not, of charged species in this class of conjugated compounds. The results from the DFT molecular geometry optimizations reported along the preceding section show that **D_3-DTT-D_3** displays an aromatic-like structure of the π-center in neutral state. However, the simulations performed for its radical anion, although not reported in detail, provide new insights into the role played by the DTT relay regarding the redox properties of the material:

(a) As for **D_3-DTT-D_3**$^{\bullet-}$, the DTT relay is predicted to bear by itself ~60% of the injected charge, while the electron-rich **D_3** groups should be less affected upon reduction. In fact, the NPA atomic charge on the bridging S atom of the π-center varies from +0.480 *e* in D_3-DTT-D_3 to +0.186 *e* in D_3-DTT-$D_3$$^{\bullet-}$, thus becoming clear the main role of this S atom not only in rigidifying the structure of the chromophore but also as drain for the storage of the injected charge. In this regard, we also notice that, within the series of compounds, the NPA atomic charge on the central S atom computed for the neutral forms of the compounds decreases from one to another at the time that the measured potential for the cathodic process increases: +0.487 *e*/−2.20 V (**D_2-DTT-D_2**), +0.485 *e*/−2.30 V (**D_1-DTT-D_1**) and +0.480 *e*/−2.35 V (**D_3-DTT-D_3**). However, it must be stressed that the atomic charge on the central sulfur atom is not fully independent of the nature of the donor end groups.

(b) There occurs an almost full reversal of the C=C/C−C conjugated backbone of the DTT spine upon the introduction of a new electron in the π-system (i.e., its four C=C bonds lengthen by ~0.020 Å, whereas the C−C bonds shorten in a similar extent), what is indicative of the attainment of a quinoid-like pattern. Furthermore, this one-electron injection further extends the rigidification of the molecule from the DTT core toward the vinylenic bridges, since the "initially double bond" still keeps upon reduction its double bond character, whereas the "initially single bond" connecting it to the DTT shortens from 1.445 Å to 1.417 Å. These molecular geometry changes lead to an enhanced degree of coplanarity between the various π-conjugated moieties with respect to the neutral compound (particularly upon solution, due to the higher energy needed to the internal rotation around the various inter-ring bonds), which in its turn facilitates the delocalization of the new electron over a larger molecular space or domain and mitigates its electrostatic repulsions with the already present π−electrons cloud.

D. Experimental and Theoretical Vibrational Spectra of Neutral Compounds. Figure 7 compares the FT-IR and FT-Raman spectral profiles of **D_3-DTT-D_3**, as the typical example for the other D-π-D chromophores studied in this paper, while the Raman spectra of the unsubstituted relay and of a DTT-containing "push−pull" chromophore are shown in Figure 8. On the other hand, Figure 9 displays a comparison between the experimental Raman profiles for **D_3-DTT-D_3** as a pure solid and in CH_2Cl_2 solution, together with its theoretical DFT// B3LYP/3-21G* spectrum.

As aforementioned in the introductory section, Raman spectroscopy can provide information about the conjugational properties of both polar (namely, push−pull) and nonpolar π-conjugated materials. Some vibrational spectroscopic observations, of general validity, which differentiate the two classes of systems are the following:

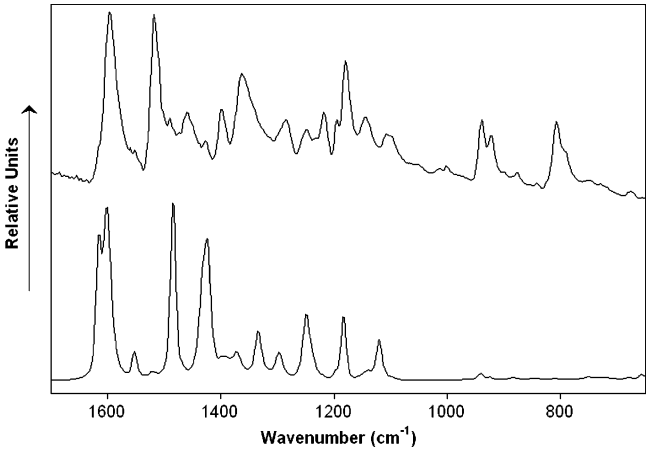

Figure 7. Comparison, over the 1700−400 cm^{-1} spectral region, between the FT-IR (upper case) and FT-Raman (lower case) spectra of **D_3-DTT-D_3**.

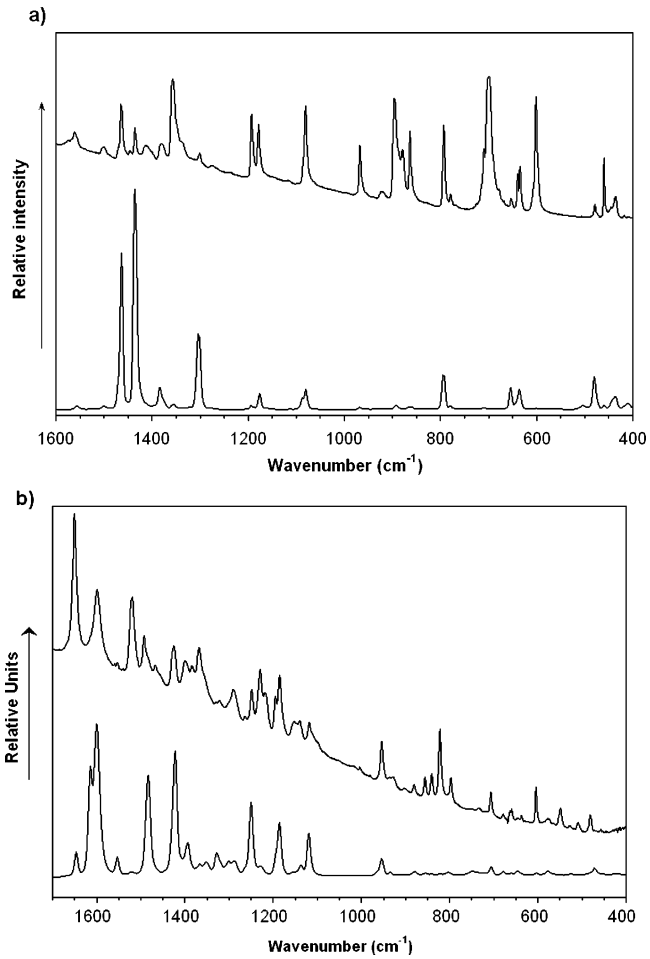

Figure 8. FT-IR (upper case) and FT-Raman (lower case) spectra in each corresponding graphic of the following: (a) unsubstituted **DTT** and (b) **D_3-DTT-CHO** as the prototypical example for a DTT-containing push−pull system.

(i) Raman spectra of nonpolar α-linked oligomers display a surprisingly simple appearance, and only three or four lines, associated to particular totally symmetric skeletal CC vibrations, are recorded with an overwhelming intensity in the 1600−1000 cm^{-1} region, as a result of the strong electron−phonon coupling, which takes place in these systems due to their quasi one-dimensional structure (see FT-Raman spectrum of **DTT** in

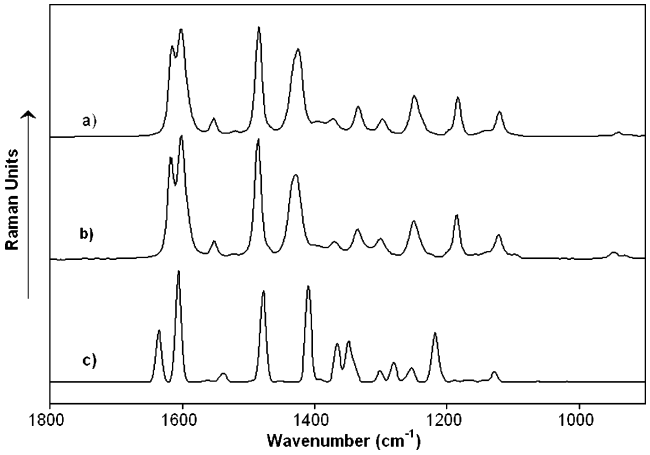

Figure 9. Comparison between the experimental FT-Raman spectral profiles of **D_3-DTT-D_3** in: (a) solid state, (b) CH_2Cl_2 solution, and (c) the theoretical DFT//B3LYP/3-21G* one.

Figure 8).[13−19] In addition, the Raman bands undergo changes in peak positions and relative intensities with the chain length of the oligomer.

(ii) On the contrary, more than three of four strong scatterings are observed in the Raman spectra of a push−pull chromophore due to the lowering of the molecular symmetry. In general, the additional lines arise from the vibrational coupling of the π-conjugating electron relay with stretching vibrations of the donor/acceptor end groups.[17,18]

(iii) The large molecular dipole moment directed from the acceptor to the donor makes the same vibrational normal modes of the π-conjugated backbone giving rise to the Raman scatterings experimentally observed to gain also an extra-large IR-activity due to the sizable fluxes of charge induced along the strongly polarized alternating sequence of double/single CC bonds (compare FT-IR and FT-Raman spectra of **D_3-DTT-CHO** in Figure 8). This is not the situation for the centrosymmetric nonpolar oligothiophenes, for which the mutual exclusion principle holds due to the existence of an inversion center in the middle of the molecule, so that Raman-active vibrations become almost undetectable in the IR spectrum, and viceversa. Furthermore, usually the out-of-plane γ(C−H) bending vibrations, appearing near 800 cm^{-1}, are by far the strongest infrared absorptions for the nonpolar oligothiophenes (see spectra of **DTT** in Figure 8). Thus, for the push−pull π-conjugated materials, the resemblance between the IR and Raman spectral profiles can be considered as a proof that an effective ICT takes place.[17,18]

Let us now proceed with the vibrational spectroscopic analysis of the compounds studied in this paper. First, we observe that despite their symmetric structure the D-π-D chromophores show some spectroscopic similarities with the class of the push−pull systems. In this regard, many IR/Raman coincidences occur for all the D-π-D systems (data for **D_1-DTT-D_1** and **D_2-DTT-D_2** are available upon request to the authors), and the Raman spectrum of **D_3-DTT-D_3** is found to be almost superposable to that of **D_3-DTT-CHO** (a system with an electronwithdrawing carbaldehyde end group), except for the scattering at 1647 cm^{-1} due to the ν(C═O) stretching which is missing in the former case. These experimental observations give further support to the existence of a partial degree of ICT in the ground-state structure of these chromophores.

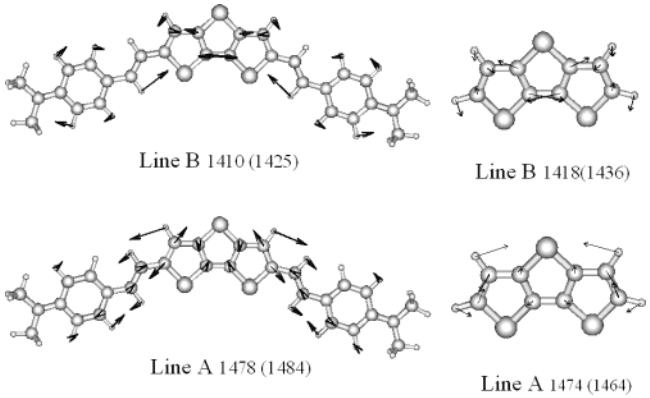

Figure 10. Selected B3LYP/3-21G* Raman-active vibrational eigenvectors for **DTT** and **D_3-DTT-D_3**. Theoretical and experimental (within parentheses) frequency values are given in cm^{-1}.

The two strongest Raman bands of **DTT** are experimentally recorded at 1464 and 1436 cm^{-1}; the former arises from a totally symmetric ν_{asym}(C═C) stretching mode of the outermost thienyl units and is related to the commonly termed as *Line A* in α-linked oligothiophenes,[12−14] whereas the second one is due to a *collective oscillation of the whole alternating sequence of C═C/C−C bonds*, along which all π-conjugated C═C bonds lengthen in-phase while all π-conjugated C−C bonds shrink in-phase, and it is denoted as the "ECC mode" or *Line B* for linear oligothiophenes[12−14] (their corresponding eigenvectors are plotted in Figure 10). The *collective skeletal mode* which gives rise to the strong Raman *Line B* mimics the change of the nuclear configuration of the π-conjugated system in passing from a *heteroaromatic*-like pattern to a *heteroquinonoid*-like one, and its frequency enables to analyze the softening of the π-conjugated backbone, along a bunch of related NLO-phores, induced by the ICT.[16,17]

Figure 9 shows the comparison between the experimental Raman spectrum of **D_3-DTT-D_3** with the DFT//B3LYP/3-21G* model one. The agreement between theory and experiments is quite satisfactory. Nonetheless, the assignment of the complete set of infrared and Raman bands of the chromophores to particular vibrational normal modes is beyond the scope of our analysis. We will restrict our discussion only to the more relevant observations of general validity for this type of D-π-D structures.

The strong Raman lines at 1615 and 1602 cm^{-1} are due to a $\nu(C{=}C)_{ring}$ stretching of the 4-*N*,*N*-dibutylaniline group extensively coupled, with different phases, to the ν(C═C) stretching of the vinylene bridges between the donor end groups and the **DTT** π-center. The large intensity of these scatterings proves the sizable contribution of the 4-*N*,*N*-dibutylaminostyryl donor groups to the overall π-conjugation of the systems.

We also observe that Raman *Line B* redshifts from 1436 cm^{-1} in unsubstituted **DTT** to 1425 cm^{-1} in **D_3-DTT-D_3**, due to the softening of the molecular backbone caused by the attachement of the donor end groups to the **DTT** spine. This frequency downshift of the "ECC mode" is in fully agreement with the predictions of the ECC model,[18] and with what experimentally found for neutral and doped oligothiophenes.[14,15] The strongest Raman scattering for the neutral (nonpolar) forms of a homologuos series of α,α'-dimethyl end-capped oligothiophenes was found to appear near 1480 cm^{-1} (being a Raman marker of a *heteroaromatic*-like pattern of the π-conjugated backbone),

whereas it largely downshifted upon oxidation of the oligomers, splitting into two components at around 1440 and 1420 cm^{-1} (which are typical markers of the attainment of a *heteroquinonoid*-like pattern of the π-conjugated path). The relative intensities of these two doping-induced Raman bands were found to be dependent on the degree of quinoidization of the π-conjugated path: that around 1440 cm^{-1} is stronger for the radical cationic species (for which the quinoidization mainly affects the inner units of the oligomer),[15a] while that near 1420 cm^{-1} becomes prominent for the dicationic species (for which the quinoidization nearly extends over the whole π-conjugated chain, due to the Coulombic repulsion between the two positive charges).[15b] This simple Raman spectral profile has also been previously found for novel classes of oligothiophene materials bearing a pure heteroquinoid structure in their electronic ground state.[23] The softening of the ECC mode for the D-π-D systems by near 11 cm^{-1} with respect to unsubstituted **DTT** agrees with the partial degree of quinoidization deduced from the net BLA values calculated for the π-center as a whole: 0.041 Å (**DTT**), 0.021 Å (**D_1-DTT-D_1**), 0.020 Å (**D_2-DTT-D_2**), and 0.021 Å (**D_3-DTT-D_3**).

Figure 9 also compares the Raman spectra of **D_3-DTT-D_3** recorded in the form of a pure solid and as solute in dilute CH_2Cl_2 solution (after properly subtracting the Raman scatterings from the solvent). We notice that the vibrational spectral fingerprints of the solute are nearly superposable to that recorded for the solid. In this regard, the major differences in peak positions of the Raman features do not exceed from a 7 cm^{-1} blueshift. We also see that the relative intensities of the most outstanding Raman features remain almost unaffected upon solution. These spectroscopic data reveal that the conjugational properties and the partial degree of ICT from the donor groups to the π-center are very little dependent on the molecular enviroment, what could be attributed to the rigid structure of DTT and its effectiveness as electron-realy[20,10] and also of the vinylenic bridges in connecting the two types of π-conjugated building blocks.[24]

E. In Situ Spectroelectrochemistry and DFT Calculations of Doped Species. Figure 11 shows the vis-NIR absorption spectra of the radical cation and dication of **D_3-DTT-D_3** (hereafter referred to as **D_3-DTT-$D_3^{+\bullet}$** and **D_3-DTT-D_3^{2+}**, respectively) recorded in situ during the slow stepwise addition of one or two equivalents of $FeCl_3$ in the CH_2Cl_2 solution. We observe that each of the subgap absorptions associated to the singly oxidized species (see schematic diagram of Figure 12) shows a well-resolved structure with two distinct components at 734−847 nm and 1312−1888 nm (two isosbestic points are also observed at 400 and 515 nm). On the other hand, as expected, the doubly oxidized species exhibits a structured NIR subgap absorption between those of the radical cation;[25] with its maximum located at 980 nm and two isosbestic points at 397 and 511 nm. Similar data were obtained by performing the oxidation process in CH_2Cl_2 solution and using iodine instead of $FeCl_3$, also in a slow stepwise manner.

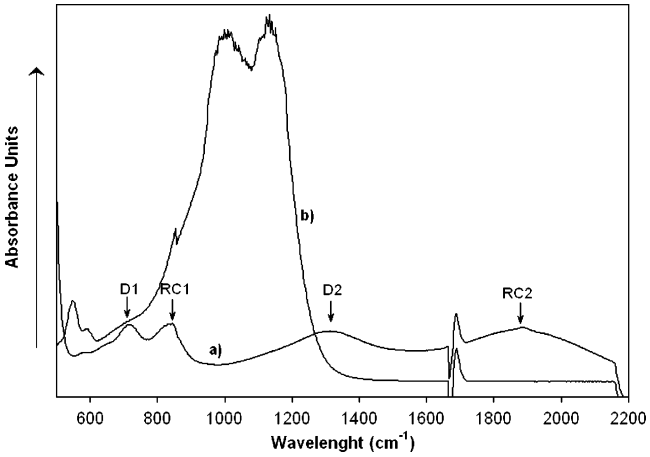

Figure 11. In situ electronic absorption spectra of the radical cation (a) and dication (b) of **D_3-DTT-D_3** after slow stepwise addition of one and two equivalents of $FeCl_3$ to the CH_2Cl_2 solution, where RC1 and RC2 denote radical cations and D1 and D2 denote π-dimers.

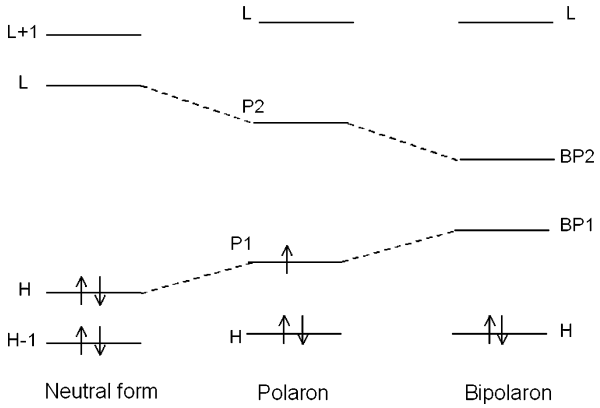

Figure 12. Schematic diagram showing the notation for the energy levels around the gap for a positively charged polaron and a positively charged bipolaron in a π-conjugated system.

It has already been shown that radical cations of oligothiophenes, oligopyrroles, mixed thiophene−pyrrole oligomers, and other polyconjugated systems usually couple into π-dimers at high concentration, low temperatures, or in polar media.[25] To investigate the nature of the "double-peaks appearance" of the doping-induced subgap absorptions we then decided to record the vis-NIR spectrum of **D_3-DTT-$D_3^{+\bullet}$** at various intermediate temperatures between 20 °C and −85 °C, and at different concentrations at room temperature. The peak at 734 nm became stronger than that at 847 nm either upon cooling or with increasing concentration of **D_3-DTT-D_3**, hence peaks denoted as RC1 and RC2 in Figure 11 correspond to (free) radical cations whereas those denoted as D1 and D2 are to be assigned to π-dimers.

We also observe that the 734 nm absorption slightly upshift upon cooling and progessively evolves into a broad feature extending to high energies, at the time that the 847 nm band becomes weaker. The evolution of the vis-NIR spectrum of **D_3-DTT-$D_3^{+\bullet}$** as the temperature goes down from −60 °C to −85 °C greatly resembles the spectral changes undergone by a thin solid film of neutral **D_3-DTT-D_3** (i.e., obtained by casting onto a quartz substrate upon solvent evaporation) during the in situ oxidation with dry iodine vapors (see Figure 13). In the latter

(23) (a) Hernandez, V.; Hotta, S.; Lopez Navarrete, J. T. *J. Chem. Phys*., **1998**, *109*, 2543. (b) Casado, J.; Miller, L. L.; Mann, K. R.; Pappenfus, T. M.; Higuchi, H.; Orti, E.; Milian, B.; Pou-Amerigo, R.; Hernandez, V.; Lopez Navarrete, J. T. *J. Am. Chem. Soc.* **2002**, *124*, 12380.
(24) Ruiz Delgado, M. C.; Hernandez, V.; Casado, J.; Lopez Navarrete, J. T.; Raimundo, J.-M.; Blanchard, P.; Roncali, J. *Chem. Eur. J.* **2003**, *9*, 3670.
(25) (a) Hill, M. G.; Mann, K. R.; Miller, L. L.; Pennau, J. F. *J. Am. Chem. Soc*. **1992**, *114*, 2728. (b) Bäuerle, P.; Segelbacher, U.; Gaudl, K.-U.; Huttenlocher, D.; Mehring, M. *Angew. Chem.* **1993**, *105*, 125. (c) Zotti, G.; Schiavon, G.; Berlin, A.; Pagani, G. *Chem. Mater*. **1993**, *5*, 620. (d) Van Haare, J. A. E. H.; Van Boxtel, M.; Janssen, R. A. J. *Chem. Mater*. **1998**, *10*, 1166.

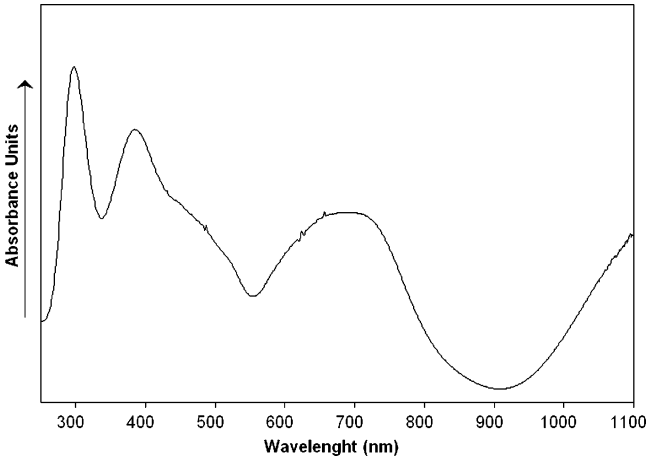

Figure 13. Solid-state vis-NIR electronic absorption spectra of the radical cation of **D_3-DTT-D_3** recorded in the form of a thin film onto a quartz substrate upon in situ exposition to dry iodine vapors.

case, a broad feature extending from 570 to 800 nm is recorded instead of the two the well-resolved double-peaks recorded in solution, being the absorbance at around 847 nm almost negligible. The onset of a second strong subgap absorption is clearly observed at around 900 nm when the oxidation is performed on the thin film, but none related doping-induced absorption is recorded below 1100 nm for the **D_3-DTT-D_3**$^{+\bullet}$ in solution. Interestingly, when the I_2-doped thin film is dissolved in CH_2Cl_2, the vis-NIR spectrum fully recovers the whole spectral profile obtained in situ for **D_3-DTT-D_3**$^{+\bullet}$ in solution (i.e., by using either I_2 or $FeCl_3$ as the oxidant agent and CH_2Cl_2 or CH_3CN as solvent). Thus, the broadening in solid state toward higher energies of the NIR subgap absorption bands of the radical cation must be ascribed to the formation of staked π-dimers.

The possibility that these double-peaks could be due to the coexistence upon oxidation of different arrangements of the constituting moieties around the vinylenic bridges (i.e., *syn*−*anti*, *anti*−*anti*, and *syn*−*syn*) with a supposedly higher interconversion energy barrier than in the pristine state because of the significant quinoid character of the inter-ring bonds was also considered. However, the ^{1}H NMR spectrum obtained after the full oxidation of the radical cation to the dication revealed again a coupling constant value of ∼14 Hz between the vinylenic hydrogens; result which supports the *anti*−*anti* conformer as the most stable one for the doped species, just like in the case of the neutral form. In addition, geometry optimizations and TDDFT calculations performed on both the *syn*−*syn* and *anti*−*anti* conformations of the radical cation and dication rendered similar changes in bond lengths and angles with respect to the neutral state and nearly the same peak positions for the doping-induced subgap absorptions (only the relative intensities of some of the vertical one-electron transitions predicted to appear in the NIR spectral region were found to slightly vary from one coplanar molecular arrangement to the another, but wavelength changes were negligible).

Calculations with the time-dependent DFT formalism were performed at the UB3LYP/3-21G* and B3LYP/3-21G* levels to assign the absorption bands observed above 400 nm for the open and closed-shell oxidized species, respectively. As reported in Table 5, there is a good agreement between theory and experiments on going from the title chromophore to the singly

Table 5. Main TDDFT//UB3LYP/3-21G* (Open-Shell Species) and TDDFT//B3LYP/3-21G* (Closed-Shell Species) Vertical One-Electron Transitions (Values in eV) to be Correlated to the Vis-NIR Absorptions Collected, Upon in Situ Stepwise Treatment With $FeCl_3$ in CH_2Cl_2 Solution for the Radical and Dication of **D_3-DTT-D_3**

redox species	experimental	theoretical	description
radical cation	1.69		π-dimer
	1.46	1.87 (f = 1.87)	P1 → P2
	0.95		π-dimer
	0.66	0.92 (f = 0.63)	H → P1 + P1 → P2
dictation	1.26	1.64 (f = 2.81)	H → BP1

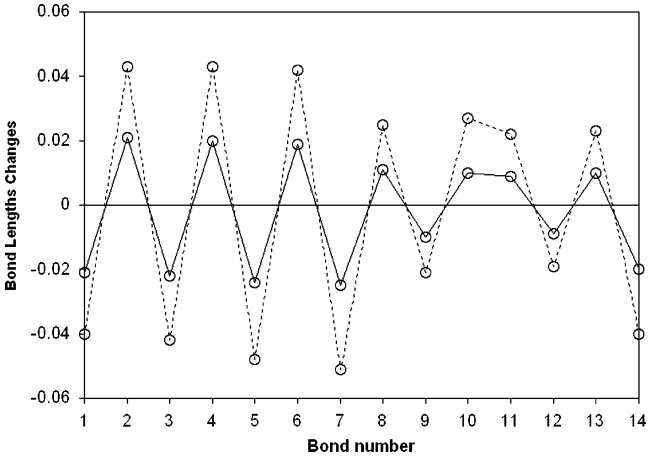

Figure 14. Theoretical changes, with respect to the neutral form, of some selected CC and CN bond lengths of **D_3-DTT-D_3** upon the generation of the radical cation (solid lines) and the dication (dashed lines). The bond numbering is the same as in Figure 1 and Table 2.

and doubly positively charged species. The assignment of the two subgap absorptions of the radical cation deserves some comments. TDDFT//UB3LYP/3-21G* calculations indicate that the mixing of the HOMO → P1 and P1 → P2 vertical one-electron excitations is moderate, the CI coefficients being 0.19 (HOMO → P1) and 0.86 (P1 → P2) for the band at higher energies; and 0.81 (HOMO → P1) and 0.45 (P1 → P2) for the second transition. Hence, the absorption at shorter wavelength is assigned as due to the excitation of the unpaired electron (α spin) from P1 to P2, whereas the band observed at longer wavelengths is due to the excitation of the β-spin from HOMO to P1. However, the mixing between excited configurations might be method-dependent since it depends on the reference wave function.

As expected, the subgap absorption band observed for the dication is to be assigned to the HOMO → BP1 excitation. Interestingly, despite the large molecular size of the chromophores there is no evidence from the DFT calculations of the formation of a "two-polaron species" in the same chain (i.e., open shell biradical dication); thus, the DFT//B3LYP/3-21G* molecular geometry of the closed shell dication (or positive bipolaron) resulted to be more stable by ∼4.8 kcal/mol than the DFT//UB3LYP/3-21G* molecular geometry of the "spin-unrestricted broken symmetry" hypothesized species.

As usually found for many types of conjugated materials, the evolution from **D_3-DTT-D_3** to **D_3-DTT-D_3**$^{+\bullet}$ and **D_3-DTT-D_3**$^{2+}$ induces significant bond-length modifications, leading to the attainment of an increased quinoid character as the number of removed π-electrons grows up (see Figure 14). The degree of quinoidization can be quantified from the BLA values

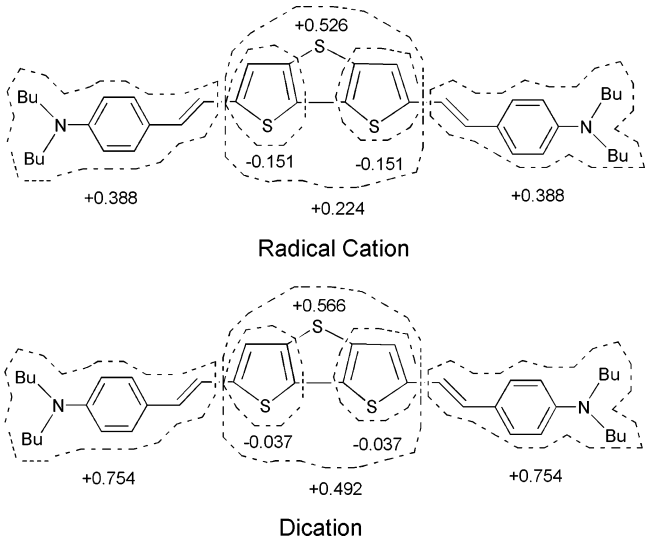

Figure 15. Overall summation (in *e*) of the natural bond orbital (NPA) atomic charges on different molecular domains for the radical cation and dication of **D_3-DTT-D_3**.

obtained for the outermost thienyl rings of the π-center (i.e., evaluated as the difference between the length of the $C_\beta C_\beta$ bond and the averaged value for the $C_\alpha C_\beta$ bonds): 0.022 Å (**D_3-DTT-D_3**); −0.021 Å (**D_3-DTT-$D_3^{+\bullet}$**); and −0.064 Å (**D_3-DTT-D_3^{2+}**). Just the same BLA value, but this time for the whole DTT relay (i.e., the overall BLA of the π-center) is obtained in each case if the optimized length of the inter-ring $C_\alpha C_\alpha$ bond is also averaged with those of the $C_\beta C_\beta$ bonds. Thus, DFT model chemistry reveals that a sizable lengthening of the $C_\alpha C_\beta$ bonds and shrinking of the $C_\alpha C_\alpha$ and $C_\beta C_\beta$ bonds occur in going from the neutral compound to the radical cation, and ultimately to the dication. From Figure 14, we see that most conjugated bonds between the two N atoms undergo similar variations in the optimized lengths upon the removal of either one or two electrons from the π-system, but 8−13 bonds belonging to the phenyl end rings experience lower changes.

Regarding the electrostatic picture of the charged species derived from their equilibrium NPA atomic charge distributions we observe, as reported in Figure 15, that for the radical cation the π-center bears a partial positive charge of +0.224 *e*, whereas the net charge over each donor group amounts to +0.388 *e* (i.e., the *N*,*N*-dibutyl-aminostyryl end moieties storage nearly the 80% of the positive charge of the radical cation). As for the dication, the corresponding values are +0.492 and +0.754 *e*, so that also in case of the doubly oxidized species the donor moeities stabilize ∼75% of the positive charge of the whole molecule.

Finally, to get a deeper experimental insight into the structural modifications taking place upon oxidation of the chromophores we have analyzed the evolution of the Raman spectrum from the neutral to the radical cationic and dicationic forms (please, compare the three spectral profiles, which are reported in Figures 7 and 16). After the removal of one electron, the strong Raman lines of **D_3-DTT-D_3** at 1615, 1602, and 1484 cm^{-1} (i.e., those scattering arising from the vibrations mostly involved in the π-conjugation of the neutral system) slightly downshift while largely weaken with respect to Raman bands at 1424 and 1334 cm^{-1}, at the time that the already existing scatterings at 1249, 1183, and 1121 cm^{-1} together with two new features at 1440 and 1071 cm^{-1} significantly gain in relative intensity (besides,

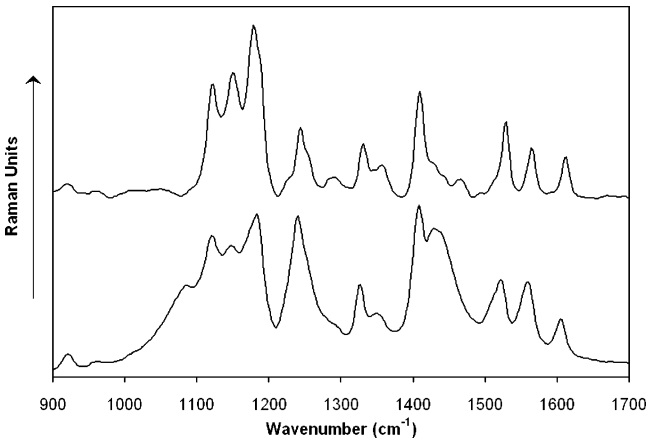

Figure 16. Raman spectral profiles for the radical cation (lower case) and dication (upper case) of **D_3-DTT-D_3**.

the 1249 and 1183 cm^{-1} lines of **D_3-DTT-D_3** slightly shift to 1237 and 1189 cm^{-1}, respectively, in passing to **D_3-DTT-$D_3^{+\bullet}$**). After double oxidation, all Raman lines become sharper, being the most outstanding scatterings now recorded at 1409 cm^{-1} and as a well-structured overlap of signals with three distinct peaks at 1180, 1150, and 1120 cm^{-1} (i.e., the prominent Raman bands are recorded at much more lower frequencies than in the neutral chromophore). On the basis of our spectroscopic intuition, the strongest Raman vibrations of the radical cation and dication are expected to mainly arise from stretching vibrations of the conjugated C═C, C−C, and C−N bonds.

To end, let us derived further information from the UB3LYP/3-21G* and B3LYP/3-21G* vibrational calculations for **D_3-DTT-$D_3^{+\bullet}$** and **D_3-DTT-D_3^{2+}**, respectively. We first note that there is a better agreement between experimental Raman frequencies and theoretical ones in the case of the dication than for the radical cation. In this regard, we would like to emphasize the following: (a) whereas the Raman spectrum of **D_3-DTT-$D_3^{+\bullet}$** was recorded in the form of a thin film in situ doped with I_2-vapors (i.e., as mentioned in the discussion of the UV−vis−NIR data), the singly oxidized species of these D-DTT-D chromophores tend to partially dimerize in solution and to π-stack in solid-state, (b) that of **D_3-DTT-D_3^{2+}** was recorded on a dilute CH_2Cl_2 solution (i.e., the electrostatic repulsions between doubly oxidized species ensure that the obtained spectrum really corresponds to single oxidized entities, just like it is assumed in the computations, and not to an overlap of scatterings from both isolated and "aggregated" species, as it is likely to occur for **D_3-DTT-$D_3^{+\bullet}$**).

Figure 17 displays the eigenvectors associated to the two skeletal vibrations of **D_3-DTT-$D_3^{+\bullet}$** and **D_3-DTT-D_3^{2+}** mostly involved in the overall π-conjugation of both doped species, and which theoretically are expected to give rise to their strongest Raman scatterings. Although coupled in some extend with ν(CC) and ν(CN) stretching motions of the donor end moieties, the vibrational displacements from their equilibrium positions taking place for the C atoms of the π-center greatly resemble those occurring for the unsubstituted **DTT** relay and neutral **D_3-DTT-D_3** along the so-termed *Lines A* and *B* (i.e., along the skeletal molecular vibrations associated to their strongest Raman scatterings measured at 1464 and 1436 cm^{-1} in the former case and at 1484 and 1425 cm^{-1} in the latter). As for **D_3-DTT-$D_3^{+\bullet}$** and **D_3-DTT- D_3^{2+}**, the four Raman normal

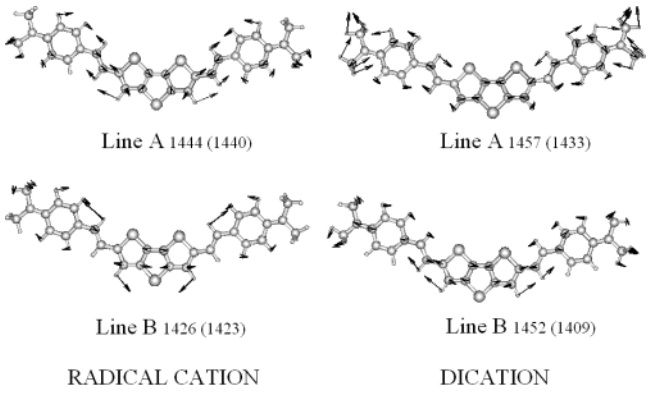

Figure 17. −Selected UB3LYP/3-21G* (radical cation) and B3LYP/3-21G* (dication) vibrational eigenvectors to be compared with the most oustanding Raman features recorded for the oxidized forms of **D_3-DTT-D_3**. Theoretical and experimental (within parentheses) frequency values are given in cm^{-1}.

modes derived from DFT model chemistry calculations and plotted in Figure 17 are to be correlated with the Raman lines experimentally recorded for the radical cation at 1440 and 1423 cm^{-1} and for the dication at 1433 and 1409 cm^{-1}. The dispersion of these characteristic Raman modes toward lower frequency values with increasing degree of quinoidization of the D-π-D chromophore contitutes a measure of the degree of softening of the π-conjugated backbone upon oxidative doping, and it is in agreement with the picture derived from the changes in BLA values between the neutral and doped species.

III. Summary and Conclusions

In this work, three symmetrical D-π-D chromophores containing dithieno[3,2-*b*:2′,3′-*d*]thiophene (DTT) as the π-center and various donor (D) end moieties have been prepared and studied by means of UV−vis−NIR and FT-Raman spectroscopy, in situ spectroelectrochemistry and quantum chemical calculations. Contrarily to what one could expect from the view of their structures and the analysis of the electrochemical behavior of short linear oligothiophenes, they display amphoteric redox properties since all exhibited two oxidations and single stable reduction peaks. We have analyzed the possible electronic modulation of the redox processes by the π-conjugated DTT relay and found that there exists a certain correspondence between the density charge on the central sulfur atom and the reduction potential, furthermore the presence of this heavy atom seems to somewhat stabilized the formation of a quinoid structure within the central spine which also helps the appearance of stable electrochemical processes. The presence of oxidations is common to oligothiophenes, nowadays we have addressed the multielectron electrochemical behavior of thesemolecules in the anodic branch which is clearly modulated by the outermost donor groups.

This work presents an attractive view of how the Raman spectra of a given family of polyconjugated molecules, either in neutral state or charged, can be suitably understood and related to their exceptional conjugated and electronic properties in the framework of the Effective Coordinate Conjugation Theory. Furthermore, it is analyzed in great detail the evolution of the conjugational properties on the basis of the optimized theoretical geometries and charges as a support to the experimental findings. In particular, the analysis of the vibrational spectra reveals some intriguing features as the similarities between the infrared and Raman spectra. Excluded symmetry reasons this optical phenomenon seems to be a consequence of the electronic polarization of the central π-conjugated linker. This effect makes the DTT to be positively charged what is in agreement with the best accommodation of new electrons in the electrochemical reduction. At the same time, the outermost donors gain certain degree of negative charge what is well related with the great dependence of the oxidations potentials with the terminal substitution of the DTT.

Our interest in the outstanding structures of the charged species on these molecules is satisfied with a detailed study of their stable oxidized species also by combining spectroscopy and theory. We have concluded the generation of radical cations and dications is greatly stabilized by the formation of quinoid structures extending over the entire system. The single oxidized molecules easily aggregate in the form of π-dimers in solution and in π-stack of π-dimers in the solid state. The analysis of the type of charged defects is a very interesting task from the point of view of the microscopic mechanism of charge fluxes taking place in real electronic and photonic devices to which the D-π-D molecules could be potentially used.

IV. Experimental and Theoretical Details

Fourier transform infrared absorption (FT-IR) spectra were recorded on a Bruker Equinox 55 spectrometer. Compounds were ground to a powder and pressed in KBr pellets. FT-IR spectra, with a spectral resolution of 2 cm^{-1}, were collected and the average of 50 scans. Interference from atmospheric water vapor was minimized by purging the instrument with dry argon before starting the data collection. FT-Raman scattering spectra were collected on a Bruker FRA106/S apparatus and a Nd:YAG laser source ($\lambda_{exc} = 1064$ nm), in a backscattering configuration. The operating power for the exciting laser radiation was kept to 100 mW in all the experiments. Samples were analyzed as pure solids in sealed capillaries and dilute CH_2Cl_2 solutions (supplied by Aldrich with analytical grade). Typically, 1000 scans with 2 cm^{-1} spectral resolution were averaged to optimize the signal-to-noise ratio. UV−vis−NIR absorption spectra were recorded either on a Lambda 19 Perkin-Elmer dispersive spectrophotometer or an Agilent 8453 instrument equipped with a diode array for a fast record of all the absorptions of the doped species appearing in the 190−1100 nm spectral region. Emission spectra were measured using a JASCO FP-750 spectrofluorometer interfaced to a Spectra Manager (v1.30.00) data station. No fluorescent contaminants were detected upon excitation in the wavelength region of experimental interest. Solutions were prepared with an absorbance between 0.1 and 0.2 at the excitation wavelength.

Cyclic voltammetry analysis was performed in CH_2Cl_2 solution (with HPLC grade). Tetrabutylammonium hexafluorphosphate (0.1 M as supporting electrolyte) was purchased from Fluka and used as received, without further purification. Solutions were deaerated by N_2 bubbling prior to each measurement, which also were run under a continuous N_2 gas flow. Electrochemical experiments were performed in a two-compartments cell equipped with a glassy carbon working microelectrode (Ø = 1 mm) and a platinum wire counter electrode. An Ag/AgCl electrode was used as reference, which was checked against ferrocene/ferricinium couple (Fc/Fc^+) before and after each experiment. Electrochemical experiments were carried out

with a Voltalab 40 potentiostat from Radiometer Copenhagen with positive feedback compensation.

Spectroelectrochemical in situ vis-NIR experiments were performed by using a homemade optically transparent thin-layer-electrode cell. The cells consists of a working electrode composed by a double sheet of ITO (transparent in the 350−2500 nm spectral range) conveniently separated by two Teflon spacers of 0.1 mm width. This separation leads to capillary ascending of the solution. The auxiliary electrode consists of a platinum grid perpendicular located with respect to the bottom part of the ITO electrode at an approximate distance of 10 mm. An Ag/Ag^+ electrode consisting of a wire between the reference and working electrodes was used as reference. The three electrodes were assembled in a Teflon stopper which at the same time covers the solution compartment (a 1 × 1 cm^2 quartz cuvette).

Density Functional Theory (DFT) calculations were carried out by means of the Gaussian 98 program[26] running on SGI Origin 2000 supercomputer. We used the Becke's three-parameter exchange functional combined with the LYP correlation functional (B3LYP).[27] It has already been shown that the B3LYP functional yields similar geometries for medium-sized molecules as MP2 calculations do with the same basis sets.[28,29] Moreover, the DFT force fields calculated using the B3LYP functional yield infrared spectra in very good agreement with experiments.[30,31] We also made use of the standard 3-21G* basis set.[32] Optimal geometries were determined on isolated entities. All geometrical parameters were allowed to vary independently apart from planarity of the rings. On the resulting ground-state optimized geometries, harmonic vibrational frequencies and infrared and Raman intensities were calculated analytically with the B3LYP functional.

We used the often-practiced adjustment of the theoretical force fields in which calculated harmonic vibrational frequencies are uniformly scaled down by a factor of 0.98 for the 3-21G* calculations, as recommended by Scott and Radom.[30] This scaling procedure is often accurate enough to disentangle serious experimental misassignments. All quoted vibrational frequencies reported along the paper are thus scaled values. The theoretical spectra were obtaining by convoluting the scaled frequencies with Gaussian functions (10 cm^{-1} width at the half-height). The relative heights of the Gaussians were determined from the theoretical Raman scattering activities.

Vertical electronic excitation energies were computed by using the time-dependent DFT (TDDFT) approach.[33,34] The twelve lowest-energy electronic excited states were at least computed for all the molecules. The computational cost of TDDFT is roughly comparable to that of single-excitation theories based on an HF ground state, such as single-excitation configuration interactions (CIS). Numerical applications reported so far indicate that TDDFT formalism employing current exchange-correlation functionals performs significantly better than HF-based single excitation theories for the low-lying valence excited states of both closed-shell and open-shell molecules.[35,36] TDDFT calculations were carried out using the B3LYP functional and the 3-21G* basis set on the previously optimized molecular geometries obtained at the same level of calculation.

Radical anions and radical cations were treated as open-shell systems and were computed using spin-unrestricted UB3LYP wave functions. The maximun value obtained for S^2 was 0.76, very close to the 0.75 theoretically expected for a doublet, showing that spin contamination is almost absent.

2,6-Bis[(9-ethylcarbazol-3-yl)vinyl]-dithieno[3,2-b:2′,3′-d]-thiophene (D_1-DTT-D_1). To the mixture of dithieno[3,2-b:2′3′-d]thiophene-2,6-dicarboxaldehyde (**DTT-2CHO**) (0.5 g; 1.98 mmol), potassium carbonate (1.37 g; 9.91 mmol), and a catalytic amount of crown ether in 40 mL of anhydrous DMF was added a 45 mL DMF solution of [(9-ethylcarbazol-3-yl)methyl]-triphenylphosphonium bromide (2.40 g; 4.36 mmol) dropwise. The solution was stirred overnight at room temperature. The resulting solution was poured into cold water dropwise to give an orange color solid precipitate, which was then filtered off and dried over P_2O_5 in a vacuum at 50 °C. The crude products were purified by column chromatography (eluent:hexane = 1:1 (v/v)), separating the monosubstituted byproduct (**D_1-DTT-CHO**) and subsequently, recrystallized from methylene chloride. The brown needle-shaped crystal (0.68 g, 54.0%) was obtained. ^{1}H NMR ($CDCl_3$): δ 8.19 (s, 2H, Ar H), 8.12 (d, 2H, Ar H), 7.63 (d, 2H, Ar H), 7.46 (m, 2H, Ar H), 7.36 (m, 4H, Ar H), 7.32−7.11 (m, 8H, Ar H), 4.36 (q, 4H, $-NCH_2CH_3$), 1.44 (t, 6H, $-NCH_2\,CH_3$). Anal. Calcd. For $C_{40}H_{30}N_2S_3$: C, 75.67; H, 4.76; N, 4.41%. Found: C, 75.41; H, 4.82; N, 4.42%.

2,6-Bis[4-(*N*,*N*-diphenylamino)styr-1-yl]-dithieno[2,3-b:2′,3′-d]thiophene (D_2-DTT-D_2). To the mixture of the compound **DTT-2CHO** (0.50 g; 1.98 mmol), potassium carbonate (0.55 g; 3.98 mmol), and a catalytic amount of crown ether was added 30 mL anhydrous DMF. A 30 mL dry DMF solution dissolving [4-(*N*,*N*-diphenylamino)benzyl]triphenylphosphonium bromide (1.19 g; 1.98 mmol) was added dropwise to the mixture solution above. After the reaction for 4 h with stirring at room temperature, the reaction mixture was poured slowly into cold water under the vigorous stirring. The orange-color precipitate was filtered off and dried under vacuum at 60 °C. Two pure products were separated by the silica gel column chromatography (methylene chloride:hexane = 1:1 (v/v)); one is monosubstituted **D_2-DTT-CHO** (0.33 g, 33.7%) and the other is disubstituted **D_2-DTT-D_2** (0.12 g). ^{1}H NMR (**D_2-DTT-CHO**, $CDCl_3$): δ 9.91 (s, 1H, −CHO), 7.90 (s, 1H, Ar H), 7.35−

(26) Frisch, M. J.; Trucks, G. W.; Schlegel, H. B.; Scuseria, G. E.; Robb, M. A.; Cheeseman, J. R.; Zakrzewski, V. G.; Montgomery, J. A.; Stratman, R. E.; Burant, S.; Dapprich, J. M.; Millam, J. M.; Daniels, A. D.; Kudin, K. N.; Strain, M. C.; Farkas, O.; Tomasi, J.; Barone, V.; Cossi, M.; Cammi, R.; Mennucci, B.; Pomelli, C.; Adamo, C.; Clifford, S.; Ochterski, G.; Petersson, A.; Ayala, P. Y.; Cui, Q.; Morokuma, K.; Malick, D. K.; Rabuck, A. D.; Raghavachari, K.; Foresman, J. B.; Cioslowski, J.; Ortiz, J. V.; Stefanov, B. B.; Liu, G.; Liashenko, A.; Piskorz, I.; Komaromi, I.; Gomperts, R.; Martin, R. L.; Fox, D. J.; Keith, T.; Al-Laham, M. A.; Peng, C. Y.; Manayakkara, A.; Gonzalez, C.; Challacombe, M.; Gill, P. M. W.; Johnson, B. G.; Chen, W.; Wong, M. W.; Andres, J. L.; Head-Gordon, M.; Replogle, E. S.; Pople, J. A. *Gaussian 98, Revision A.7*; Gaussian Inc.: Pittsburgh, PA, 1998.
(27) Becke, A. D. *J. Chem. Phys.* **1993**, *98*, 1372.
(28) Stephens, P. J.; Devlin, F. J.; Chabalowski, F. C. F.; Frisch, M. J. *J. Phys. Chem.* **1994**, *98*, 11623.
(29) Novoa, J. J.; Sosa, C. *J. Phys. Chem.* **1995**, *99*, 15837.
(30) Scott, A. P.; Radom, L. *J. Phys. Chem.* **1996**, *100*, 16502.
(31) Rauhut, G.; Pulay, P. *J. Phys. Chem.* **1995**, *99*, 3093.
(32) Pietro, W. J.; Francl, M. M.; Hehre, W. J.; Defrees, D. J.; Pople, J. A.; Binkley, J. S. *J. Am. Chem. Soc.* **1982**, *104*, 5039.
(33) Runge, E.; Gross, E. K. U. *Phys. Rev. Lett.* **1984**, *52*, 997. Gross, E. K. U.; Kohn, W. *Adv. Quantum Chem.* Gross, E. K. U., Driezler, R. M., Eds.; Plenum Press: New York, 1995; p 149.
(34) Casida, M. E. *Recent Advances in Density Functional Methods, Part I.;* Chong, D. P., Ed.; World Scientific: Singapore, 1995; p 115.
(35) Koch, W.; Holthausen, M. C. *A Chemist's Guide to Density Functional Theory;* Wiley-VCH: Weinheim, 2000.
(36) Casado, J.; Miller, L. L.; Mann, K. R.; Pappenfus, T. M.; Kanemitsu, Y.; Ortí, E.; Viruela, P. M.; Pou-Amérigo, R.; Hernandez, V.; López Navarrete, J. T. *J. Phys. Chem. B* **2002**, *106*, 3872.

7.20 (m, 5H, Ar H), 7.19−6.92 (m, 12H, Ar H). ^{1}H NMR (**D_2-DTT-D_2**, $CDCl_3$, ppm): δ 7.33 (d, 4H, Ar H), 7.25 (m, 8H, Ar H), 7.14−7.08 (m, 12H, Ar H), 7.05−7.01 (m, 8H, Ar H), 6.85 (d, 2H, Ar H). Anal. Calcd. For $C_{48}H_{34}N_2S_3$: C, 78.44; H, 4.66; N, 3.81%. Found: C, 78.30; H, 4.77; N, 3.82%.

2,6-Bis[4-(*N*,*N*-dibutylamino)styr-1-yl]-dithieno[2,3-b:2′3′-d]thiophene (D_3-DTT-D_3). To the suspension of 4-(*N*,*N*-dibutylbenzyl)triphenyphosphonium iodide (0.729 g; 1.2 mmol) and potassium ter-butoxide (0.27 g; 2.4 mmol) in 60 mL methylene chloride were added 18-crown-6 ether (10 mg) and **DTT-2CHO** (0.30 g; 1.2 mmol) under vigorous stirring at room temp. The reaction was completed within two hrs. The reaction mixture was filtered through diatomaceous earth to eliminate the crown ether. After evaporating the solvent from the filtrate, the product mixtures were separated by silica gel chromatography using methylene chloride as eluent. While the monosubstituted byproduct (**D_3-DTT-CHO**) crystallized readily from the solution, the di-substituted product (**D_3-DTT-D_3**) was difficult to crystallize so that needed another chromatography for further purification. After evaporation of the solvent, the residue was dissolved in *n*-heptane and obtained as a crystalline product. The pure product was dried at 40 °C under vacuum (yielding 0.13 g). ^{1}H NMR (**D_3-DTT-D_3**, $CDCl_3$): δ 7.33 (d, 4H, Ar H), 7.09 (s, 4H, Ar H), 6.93 (m, 4H, −CH═CH−), 6.20 (d, 2H, Ar H), 3.29 (t, 4H, CH_2N), 1.54(m, 8H, CH2(CH_2N)). Anal. Calcd. For $C_{40}H_{50}N_2S_3$: C, 73.35; H, 7.69; N, 4.28%. Found: C, 72.98; H, 7.53; N, 4.27%.

Acknowledgment. The authors are very grateful to Professor Jean Marie Lehn for his fruitful discussions. R.P.O., M.C.R.D., J.C., V.H., and J.T.L.N. would like to acknowledge the Dirección General de Enseñanza Superior (DGES, MEC, Spain) for financial support to the investigation performed at the University of Málaga through projects BQU2000-1156 and BQU2003-03194. The research was also supported by the Junta de Andalucía (Spain) under grant FQM-0159. J.C. thanks the (MCyT) for a "Ramón y Cajal" position of chemistry at the University of Málaga. M.C.R.D. and R.P.O. also thank the Ministerio de Educación y Ciencia (MEC) of Spain for personal grants. O.K.K. is grateful for partial funding support from DARPA, AFOSR and Office of Naval Research.

JA047058O